

Local density of state fluctuations in 2d multifractal superconductor

Mathieu Lizee,^{1,2} Matthias Stosiek,³ Christophe Brun,² Igor Burmistrov,^{4,5} and Tristan Cren²

¹*Laboratoire de Physique de l'École Normale Supérieure, ENS, Université PSL, CNRS, 3 Sorbonne Université, Université Paris Cité, 75005 Paris, France*

²*Institut des Nanosciences de Paris, Sorbonne Universités, UPMC Paris, France*

³*Physics Division, Sophia University, Chiyoda-ku, Tokyo 102-8554, Japan*

⁴*L. D. Landau Institute for Theoretical Physics, acad. Semenova av. 1-a, 142432 Chernogolovka, Russia*

⁵*Laboratory for Condensed Matter Physics, HSE University, 101000 Moscow, Russia*

The interplay of superconductivity and disorder is known to generate a wealth of new phenomena which have driven the history of superconductivity since its infancy. One of the major breakthroughs in the field was the celebrated quantum phase transition from superconductor to insulating state. Interestingly, the opposite effect has been reported several times : an increase of the superconducting critical temperature by disorder. One of the proposed mechanisms involves the peculiar structure of diffusive electronic wavefunctions whose multifractality can increase the superconducting pairing. Recent experiments in monolayer NbSe₂ on graphene have reported T_c enhancement due to multifractal superconductivity but the field-theoretical models at our disposal fail to account for this effect at the relevant level of disorder. In this work, we use an epitaxial monolayer of lead showing a simple band structure and homogenous structural disorder as a model system of a 2d multifractal superconductor in the weak-antilocalization regime. Then, we perform an extensive study of the emergent fluctuations of local density of states in this material and compare them with both analytical results and numerical solution of the attractive Hubbard model. We show that mesoscopic LDOS fluctuations allow to probe locally elastic scattering and dephasing rate in 2d weakly disordered materials in particular in the most interesting multifractal regime.

I. INTRODUCTION

Since the seminal paper by Anderson, the field of wave localization in disordered media has developed immensely. In the metallic regime, mesoscopic fluctuations of conductance have been observed in a wealth of condensed matter systems signaling the diffusion of electrons in a quenched disorder potential and are commonly referred to as the ‘weak localization’ signature. Although a similar signature of weak localization is predicted to emerge in maps of local density of states (LDOS) and several groups have reported LDOS spatial fluctuations [1–3], their understanding in diffusive materials remains elusive especially on the experimental side.

Another major problem of condensed matter physics is the interplay of interactions and disorder. Not only are these questions at the heart of the many-body localization problem but they have also grown central in the field of disordered superconductors [4, 5]. Indeed, the pairing of weakly localized ‘multifractal’ electrons is predicted to yield a disorder-enhanced T_c compared to the clean metal case in well chosen conditions [6, 7]. Recently, a first experimental demonstration of a possible multifractal enhancement of T_c in NbSe₂ monolayers has been reported [3]. A deeper understanding of 2d diffusive superconductors in the multifractal regime is now required to strengthen this discovery and stimulate the engineering of multifractally enhanced superconductors. Indeed, not only is NbSe₂/graphene a complex material challenging to tackle numerically but the nature of disorder used in this study (random sulphur or silicon atom substitution) along with its own non trivial spatial structures raises significant issues. Thus, the need for an un-

derstanding of multifractal superconductivity and especially in the weak-antilocalization regime of NbSe₂ calls for new model systems.

In this study, we probe the mesoscopic fluctuations of LDOS in a purely two-dimensional weakly disordered superconductor with high resolution scanning tunneling spectroscopy. We prove quantitatively that weak disorder effects on diffusive electrons control the LDOS fluctuations close to the superconducting coherence peak. To generalize our interpretation, we compare our measurements with self-consistent solutions of the attractive Hubbard model on state of the art system size [8, 9]. We report the first measurements of LDOS correlations in weakly disordered 2d superconductors and demonstrate that the energy dependency of mesoscopic LDOS fluctuations allows to extract the effective scattering rate of low energy single particle excitations. Finally, our work provides a new toolbox for the study of multifractal superconductivity in 2d systems which remains a huge challenge to the theoretical approaches.

II. EXPERIMENTS

As model systems for the study of two-dimensional weakly disordered electronic systems, epitaxial monolayers of metals on semiconducting surfaces are exceptionally interesting. Firstly, their thickness of the order of the Fermi wavelength along with their good decoupling from the bulk makes them truly two-dimensional. Secondly, they show a wealth of phases with highly uniform and reproducible structural disorder without the need to evaporate chemical contaminants on the sample. Thus, these

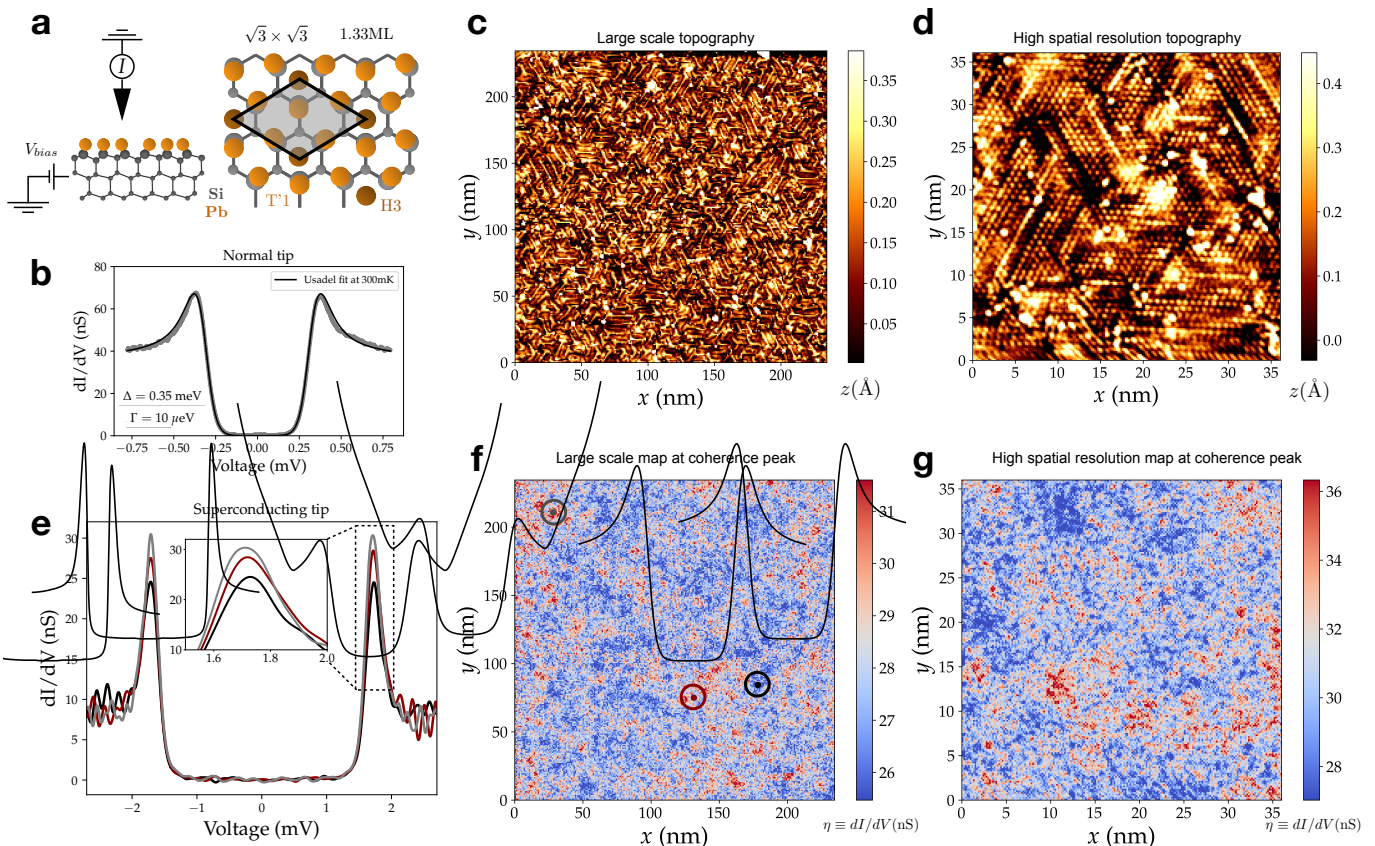


FIG. 1. Tunneling conductance fluctuations in the stripped incommensurate (SIC) phase of lead on Si **a** Description of the scanning tunneling spectroscopy measurement and of the SIC phase (1.33 ML of Pb/Si with $\sqrt{3} \times \sqrt{3}$ symmetry). On **b**, we show the tunneling conductance of the SIC phase measured with a platinum tip along with the best fit with the Usadel formula (see Appendix A). We find $\Delta_{\text{SIC}} = 0.35$ meV and $\Gamma_{\text{SIC}} = 10$ μeV . **c** Topographic image of the SIC monolayer phase. One clearly sees the rotational nanodomains of the $\sqrt{3} \times \sqrt{3}$ phase separated by domain walls made of the $\sqrt{7} \times \sqrt{3}$ reconstruction. An atomically resolved image is shown in **d**. In **e**, several differential conductance spectra (dI/dV) measured at the positions shown on **f** are presented. On **f**, the isoenergy map corresponding to topography **c** at the coherence peak energy $V_{\text{max}} = 1.7$ meV is shown. Symmetrically, on **g**, we show the iso-energy dI/dV map corresponding to topography **d** at the same bias voltage.

systems fully fabricated in ultra-high-vacuum are exceptionally clean and homogeneously disordered in contrast with the usually studied substitution alloys [1–3] where the disorder itself already has long range correlations as shown on topographic maps of references [2, 3]. In this work, we chose to work on the stripped incommensurate (SIC) phase of lead on silicon. The ideal SIC monolayer described in Figure 1a is made of 1.33 monolayer of lead atoms on top of a Si(111) surface. The lead is evaporated on the 7×7 reconstruction of silicon in-situ a home made scanning tunneling microscope. The SIC phase is made of nanometric domains oriented preferentially along 3 directions as shown on large scale in Figure 1c and with atomic resolution in Figure 1d. The sample is then cooled to 300 mK, well below its critical temperature of 1.8 K. On panel **b**, we show the tunneling spectroscopy at 300 mK measured with a platinum (flat DOS) tip. The solid line is a solution of the Usadel equation for diffusive superconductors (mean free path is much smaller than su-

perconducting coherence length) [10] (see Appendix A). The SIC phase is found to have a gap of $\Delta_{\text{SIC}} = 0.35$ meV and a depairing energy of $\Gamma_{\text{SIC}} = 10$ μeV . In order to probe the mesoscopic fluctuations of this phase, we acquire a large scale (250 nm x 250 nm) spectroscopic map with nanometric spatial resolution. A superconducting tip (bulk lead) is used to increase the energy resolution to 30 μeV [11, 12]. The dI/dV spectrum (Fig. 1e) shows sharp coherence peaks at $V_{\text{max}} \sim \Delta_{\text{tip}} + \Delta_{\text{SIC}} = 1.7$ mV in agreement with the known gap of the SIC phase $\Delta_{\text{SIC}} \sim 0.35$ mV. Three individual spectra whose positions are shown in **f** are displayed in **e**. These spectra demonstrate that conductance fluctuations are stronger at the coherence peak and do not indicate large variations of the peak's position E_{max} or in other words the gap width Δ as expected in the weak disorder regime. Displaying the local differential conductance at a given bias voltage V_{bias} yields iso-energy dI/dV maps. On Figure 1f, we show the dI/dV map measured at the en-

ergy of the coherence peak (1.7 mV) and evidence spatial fluctuations of the differential conductance at various scales. An interesting feature of this map is indeed that no characteristic scale of the domains can be easily identified. This fractal-like property is reminiscent of criticality close to the Anderson transition and suggests a weak-localization-like phenomenology. Considering the nanometric scale structure of the monolayer, we also acquire a high resolution map of 35 nm in order to better capture small scale fluctuations. On Figure 1d and g, we show respectively the topographic and spectroscopic (at the coherence peak) high resolution map. The tunneling conductance shows strong spatial fluctuations spanning many scales below the superconducting coherence length $\xi \sim 50$ nm [11, 12]. The obvious lack of correlation to structural disorder (topography) leads us to attribute these emergent fluctuations to coherent diffusion.

III. FLUCTUATION ANALYSIS

In order to probe superconducting properties in more details, we focus LDOS spatial variance close to the superconducting coherence peak. At voltage V , the variance of iso-energy tunneling conductance maps (shown on Figure 2a for $V \in \{1.5, 1.6, 1.7, 2\}$ mV) writes $\sigma_{\text{exp}}^2(V) = \langle \delta \frac{dI}{dV} \rangle_r$ where to keep notations light, $\eta = dI/dV$ denotes the differential conductance and the brackets denote spatial averaging. On Figure 2b, we plot (in green) the variance $\langle \delta \eta^2 \rangle$ as a function of bias voltage, showing a maxima close to the coherence peak energy $V_{\text{max}} = E_{\text{max}} + \Delta_{\text{tip}} = 1.7$ mV in agreement with the qualitative observation we made earlier (*cf.* Figure 1e) that fluctuations are higher at the coherence peak.

A. Theoretical predictions

To rationalize the energy dependency of LDOS spatial variance, we now compute the fluctuations of den-

sity of states in a two-dimensional diffusive superconductor. In the following, we sketch a simplified derivation of the density of states correlator in diffusive superconductors. We have $\rho(E, r) = -\frac{1}{\pi} \text{Im} G^R(E, r, r)$ with $G^R(E, r, r) = \langle r | \frac{1}{E - H + i\eta} | r \rangle$. Like in the mean-field solution to the BCS Hamiltonian, we introduce the Bogoliubov operators and coherence factors u_α and v_α associated to the single particle eigenstates ϕ_α for the eigenvalue ϵ_α , solutions of the single particle Schrödinger equation including the disordered potential. The LDOS can be written conveniently as:

$$\rho(E, r) = \sum_{a, s=\pm} \phi_a^2(r) (1 + \epsilon_a/E) \delta(E - s\sqrt{\epsilon_a^2 + \Delta^2}) \quad (1)$$

The density of states correlations are then computed from this expression along with the dynamical structure factor which is a spatially averaged product of wavefunctions measured at position \mathbf{r} and \mathbf{r}' and at well determined energies. If one neglects the dependency of single particle density of states on energy in the normal state, this structure factor can be computed from the polarization operator $\Pi^R(\omega, \mathbf{r}, \mathbf{r}')$

$$F(\epsilon, \omega, \mathbf{r}, \mathbf{r}') = \frac{1}{\pi\omega} \text{Im} \Pi^R(\omega, \mathbf{r}, \mathbf{r}') \quad (2)$$

In the *diffusive regime at weak disorder*, one gets for the Fourier transform of the polarization operator

$$\Pi^R(\omega, \mathbf{q}) = \rho_0 \frac{Dq^2}{Dq^2 - i\omega}, \quad (3)$$

where D denotes the diffusion coefficient and ρ_0 the density of states of the non interacting problem at the Fermi level. The full derivation then yields the pair LDoS correlation function at different points (r_1, r_2) and different energies (E_1, E_2) [9]:

$$\begin{aligned} \langle \delta\rho(E_1, \mathbf{r}_1) \delta\rho(E_2, \mathbf{r}_2) \rangle &= \frac{\rho_0^2}{2\pi g} \Re \left\{ \left[1 + X_{E_1} X_{E_2}^* \right] K_0 \left(R \sqrt{\frac{2\gamma_\Phi - iE_1/X_{E_1} + iE_2/X_{E_2}^*}{\hbar D}} \right) \right. \\ &\quad \left. - \left[1 - X_{E_1} X_{E_2} \right] K_0 \left(R \sqrt{\frac{2\gamma_\Phi - iE_1/X_{E_1} - iE_2/X_{E_2}}{\hbar D}} \right) \right\} \quad (4) \end{aligned}$$

where $R = |\mathbf{r}_1 - \mathbf{r}_2|$, K_0 stands for the modified Bessel function. Also, we introduce $X_E = E/\sqrt{E^2 - \Delta_E^2}$ where we phenomenologically substitute Δ by the complex energy dependent gap-function Δ_E which can be computed analytically [13] for weakly disordered 2d superconduc-

tors. To compare Eq.(4) with experiments, X_E is estimated using the Usadel model for diffusive superconductors. As detailed in Appendix A, we find a gap $\Delta_{\text{SIC}} = 0.35\text{meV}$ and a depairing energy $\Gamma_{\text{SIC}} = 10\mu\text{eV}$. Finally, two parameters control the strength of density of state

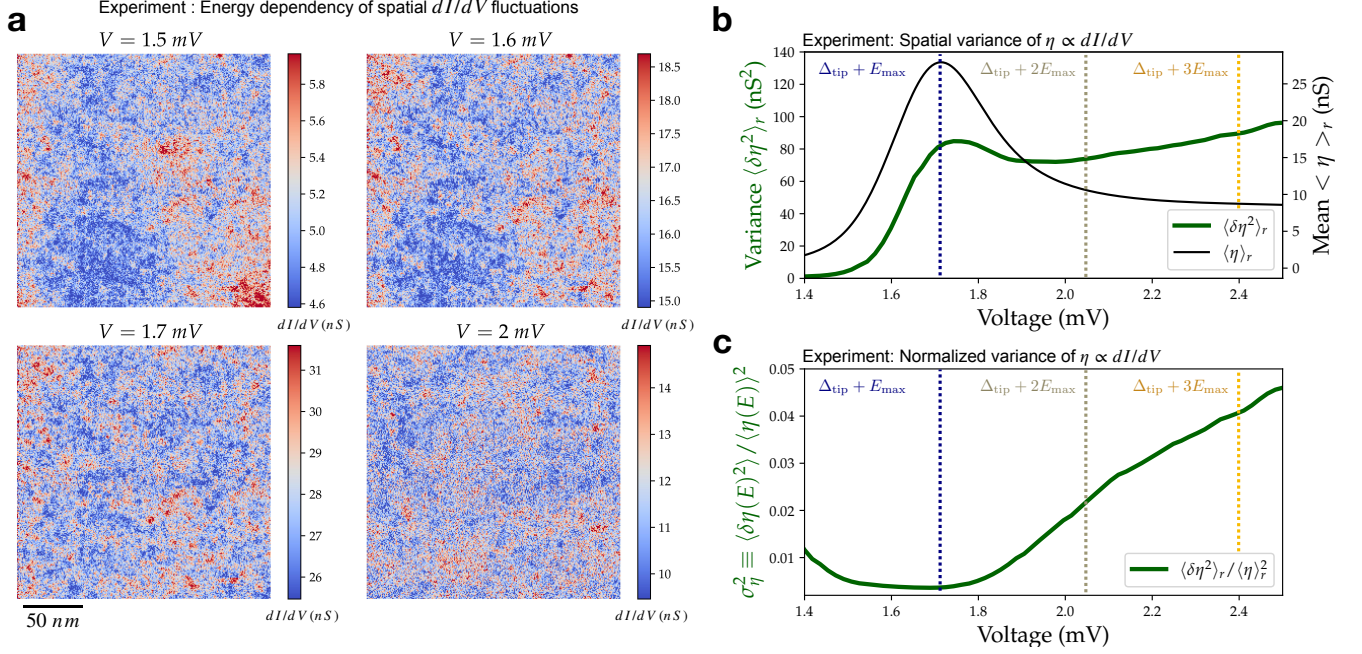


FIG. 2. **Analysis of tunneling conductance fluctuations** **a** Iso-energy maps of the differential conductance $\eta = dI/dV$. **b** Variance (green) and mean value (black) of the tunneling conductance computed on iso-energy maps as a function of the bias voltage. On **c**, we show the bias voltage dependency of the normalized variance $\sigma_{\text{exp}}^2 = \langle \delta\eta(V)^2 \rangle / \langle \eta(V) \rangle^2$ (green).

fluctuations: the dimensionless conductivity $g = hD\rho_0/2$ and the effective dephasing rate $\gamma_\Phi = \hbar D/L_\Phi^2$, assumed to be energy independent in this calculation. On Figure 3a, we show the energy dependency of the density of states normalized variance $\sigma_\rho^2(E) = \langle \delta\rho(E)^2 \rangle_r / \langle \rho(E) \rangle_r^2$. Here, the conductance is fixed at $g = 30$ and we show the plots for several values of γ_Φ ranging typically between $\Gamma \sim k_B T \sim 30\mu\text{V}$ and $\Delta \sim 350\mu\text{V}$. In black, we show the mean density of states spectrum ($\Re(X_E)$) used for this computation, namely the best Usadel fit for the SIC phase (see Appendix A). We show that σ_ρ^2 has a local minimum close to the coherence peak energy E_{max} , in good agreement with the minimum of normalized variance σ_{exp}^2 at the superconducting coherence peak on Figure 2c. On panels **b,c**, we show that at fixed energy, σ_ρ^2 decreases with increasing conductivity (as expected from the $1/g$ dependency in equation (4)). On panels **b,d**, we show that increasing dephasing rate γ_Φ corresponding to smaller system size in a transport experiment decreases the variance σ_ρ^2 . We stress that these dependencies are very much expected from the understanding of mesoscopic fluctuations. Larger electronic phase coherence length and lower conductance lead to enhanced fluctuations, whether one measures conductance or LDOS fluctuations.

B. Electronic diffusion in the SIC phase and quantitative extraction of transport parameters

In order to strengthen our analysis and compare precisely experiment with theoretical predictions, we evaluate the diffusion coefficient in the SIC phase by independent means. We refer to previous work by some of the authors where the proximity effect between the SIC phase and small bulky lead islands allowed to estimate the diffusion coefficient of the monolayer [11]. These results are supported by another measurement where the spatial profile of a vortex core allowed us to extract the dirty coherence length and thus the electronic diffusion coefficient [12]. Both these measurements yield a dirty coherence length $\xi \in [45, 50]$ nm. Writing $\xi = \sqrt{\hbar D/\Delta}$ with $\Delta_{\text{SIC}} = 0.35$ meV gives a diffusion coefficient $D \in [10, 15]$ cm²/s. We now consider the Einstein relation for the conductivity (per spin orientation) of the monolayer $g = hD\rho_0/2$ and write the density of states of a two-dimensional electron gas $\rho_0 = 2 \frac{k_F}{\hbar v_F} = \frac{2m}{2\pi\hbar^2}$ (factor of 2 for the two spin orientations). This leaves us with $g = \frac{mD}{\hbar}$. Using the known effective mass $m = 1.27 m_e$ in the SIC phase [14], we can estimate $g \sim 20$. We insist that this value may be under-estimated as in proximity effect experiments, the bulk lead islands could act like additional scattering centers (spaced by ~ 10 nm) which are absent in the present structurally optimized SIC monolayer. Thus we infer that $g = 20$ is in fact a lower bound of the actual conductance and we roughly estimate $g \in [20 - 100]$.

Theory for LDOS spatial fluctuations

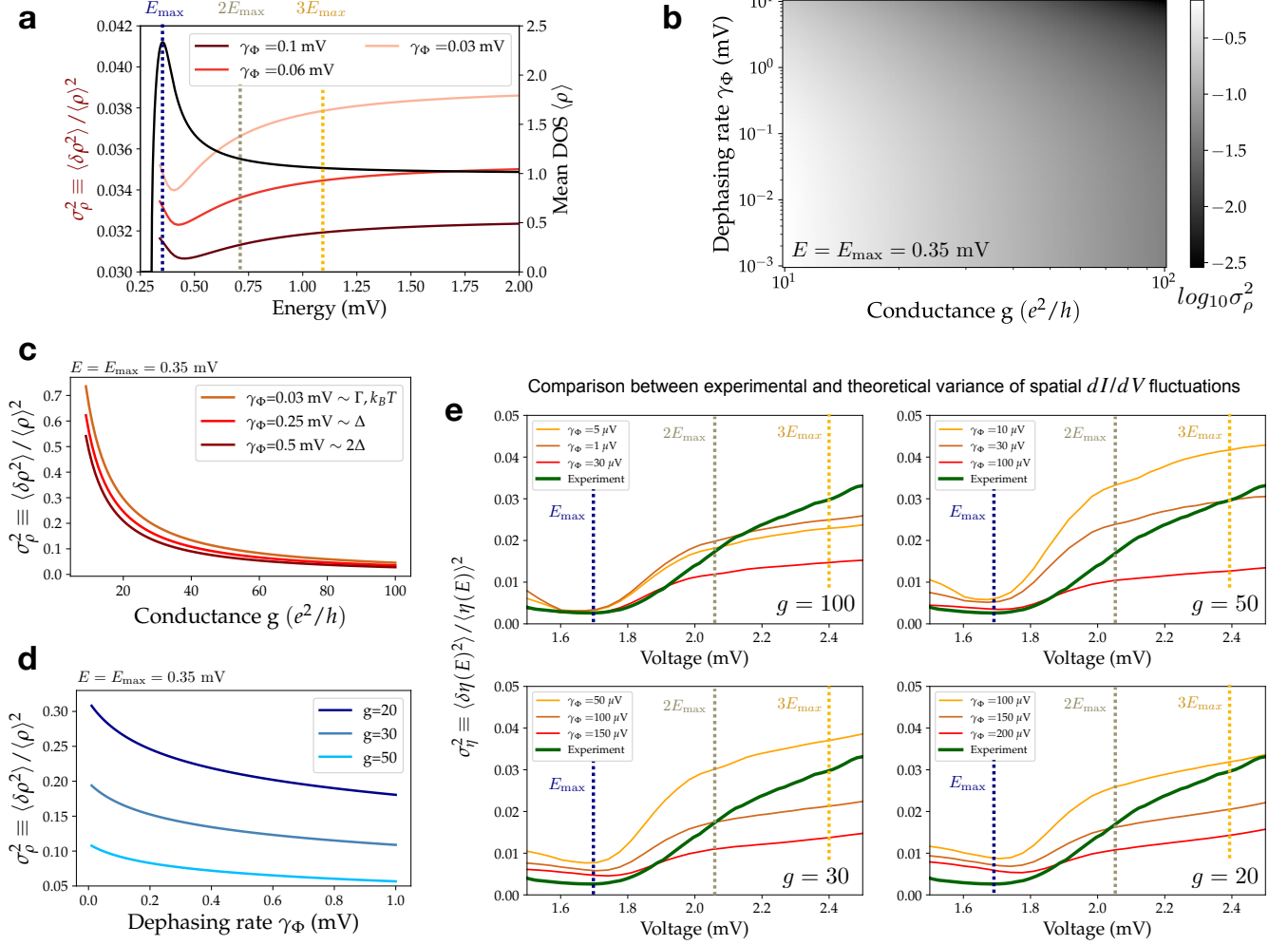


FIG. 3. **Analysis of tunneling conductance fluctuations** On panels **a-d**, we describe the fluctuations of density of states computed semi-analytically as a function of energy E , conductance g and effective dephasing rate γ_Φ . On **a**, we show the energy dependency of the normalized variance σ_ρ^2 (red) at $g = 30$ and several values of $\gamma_\Phi \in \{0.03, 0.06, 0.1\}$ mV. In black, we show the mean density of states used for the calculation (solution of Usadel equation, *cf* Appendix A). On **b-d**, we now fix the energy at $E_{\max} = 0.35$ mV and plot on **b** a color-map the log of σ_ρ^2 as a function of both conductance and dephasing rate. On **c**, we show the dependency of σ_ρ^2 on conductance for $\gamma_\Phi \in \{0.03, 0.25, 0.5\}$ mV. On **d**, we show the dependency on dephasing rate for $g \in \{20, 30, 50\}$. On **e**, we compare the experimentally measured normalized variance of tunneling conductance σ_η^2 with the one computed semi-analytically from density of states correlations (Eq.(13) derived in Appendix D from Eq.(4)). We plot the theoretical prediction for $g \in \{20, 30, 50, 100\}$ and the levels of dephasing which best reproduce the experimental data in each case. We stress that no free parameter is used here.

C. Comparison with experiments

We now attempt a quantitative comparison of our theoretical analysis with our experiments on the SIC phase of lead on silicon. Using equations Eq. (4), we compute the normalized variance of the tunneling conductance: $\sigma_\eta^2 = \langle \delta\eta(V)^2 \rangle_r / \langle \eta(V) \rangle_r^2$ at a bias voltage V . Here, we take into account the tip density of states and variations of the tip height above the sample during the measurement. All details are given in Appendix B. The formula we obtain for σ_η^2 (Eq. (13)) is a simple energy integration

of the density of states correlator given in equation (4).

The tunneling conductance variance can then be compared to the experimentally measured σ_{exp}^2 (in green) on Figure 3e. The thin lines are semi-analytical calculations of σ_η for $g \in \{20, 30, 50, 100\}$ from Eq. (13). For each value of g , we plot the theoretical curve for a few dephasing rates γ_Φ which best reproduce the experimental variance. We stress that no free parameter is used here as g takes very reasonable values for the SIC phase [11, 12] while the dephasing rate γ_Φ is constrained in a rather narrow window of physically relevant energies $\gamma_\Phi \in [1, 150] \mu\text{eV} \sim [k_B T / 30, \Delta_{\text{SIC}} / 2]$. We obtain an ex-

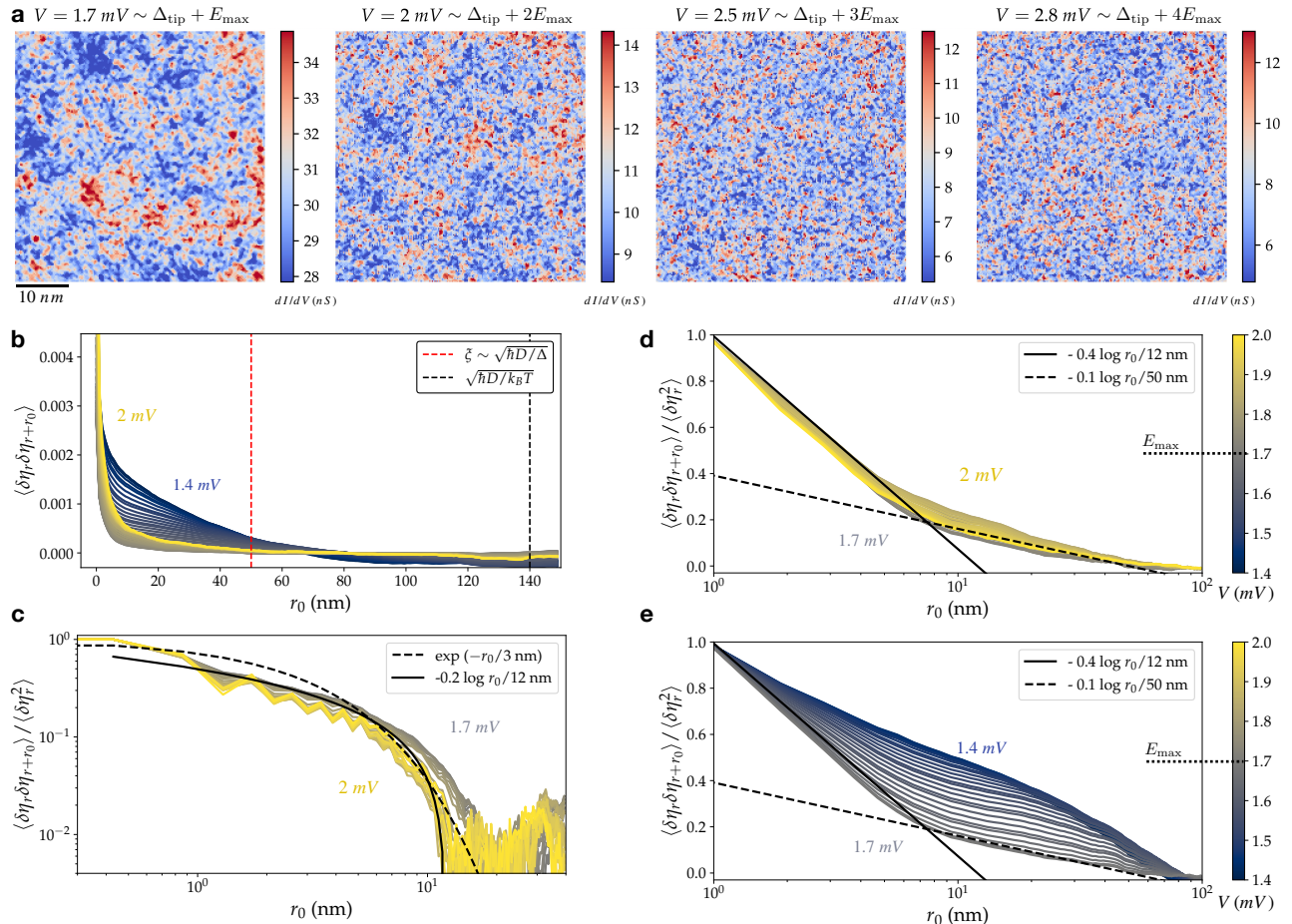


FIG. 4. **dI/dV spatial correlations** On **a**, we show several iso-energy high resolution differential conductance maps for $E = V - \Delta_{\text{tip}} \in \{1, 2, 3, 4\} E_{\text{max}}$. On panel **b**, we show the angle averaged 2-point correlations on large scale maps as a function of distance and bias voltage (color scale for panels **b-e** given on panels **d,e**). On this plot, we also show the position of superconducting coherence length ξ (red) and the diffusion length corresponding to energy scale $k_B T \sim 30 \mu\text{eV}$ (black). On **c**, we plot the angle averaged auto-correlation computed on small scale maps. On **d,e**, we use lin-log scales to evidence the peculiar behavior of the auto-correlation (normalized by its zero distance value). On **d**, we focus on energies below E_{max} and on **e**, on energies above E_{max} .

cellent quantitative agreement between experiment and theoretical predictions for a range of parameters corresponding to $g \in [50, 100]$ where the energy dependency of the normalized variance close to the coherence peak is very nicely reproduced.

Thus, we claim that emergent dI/dV spatial fluctuations in the 2d superconductor are a direct probe of coherent diffusion, well reproduced by a simple analytical model (section III A). Although a quantitative extraction of γ_Φ is difficult in our case, our results show that in contrast with transport measurements, scanning tunneling spectroscopy intrinsically allows for a local measurement of both dimensionless conductance and electronic coherence length far from step edges or contacts, through direct probe of electronic diffusion in the material.

IV. SPATIAL CORRELATIONS

After considering the variance of the iso-energy maps and thus disregarding the spatial structure of dI/dV fluctuations, we briefly focus on the analysis of spatial correlations of the local conductance: $\langle \delta\eta_r \delta\eta_{r+r_0} \rangle_r$. On Figure 4 **a**, we show several high resolution conductance maps at various energies above the coherence peak $E = V - \Delta_{\text{tip}} \in \{0.35, 0.7, 1.2, 1.5\} \text{ mV} \sim \{1, 2, 3, 4\} E_{\text{max}}$. We observe very clearly that large scale spatial structures at E_{max} tend to disappear with increasing energy.

To explore the iso-energy spatial correlations of tunneling conductance, we plot on Figure 4**b** the angle-averaged 2-point correlation function as a function of distance r_0 .

The color of the curve represents the energy at which it is measured. On **c**, we use a log-log representation of the auto-correlation function on high resolution maps (normalized by its value at 0.1 nm). To better show the angle averaged radial decay at various energies on large scale 250 nm maps, we normalize the auto-correlation by its value at $r_0 = 1$ nm and plot them for energies below E_{\max} on Figure 3d and above E_{\max} on Figure 3e where the curve's color is coding its energy below 1.4 and 2 mV. It is apparent here that above E_{\max} , these auto-correlation profiles depend only very weakly on energy. On **e**, we show that the spatial auto-correlation has a short range regime with steep decay up to approximately 10 nm followed by a long range regime with a slower decay. As made visible with the black lines, two apparently log-decay regimes are identified with characteristic distance slopes of 12 and 50 nm for the short and long range regimes respectively. The fact that these two characteristic lengths appear in the autocorrelation function seems very natural as 10 nm correspond to the average nanocrystal size of the SIC monolayer and 50 nm to its superconducting coherence length.

To deepen our understanding of these LDOS fluctuations, we use a numerical model of a superconducting electrons on a 2d disordered lattice in the weak disorder regime. The deep similarity between experimental and fully self-consistent tight-binding models then allow us to gain important insights through comparison with the analytical theory of weakly disordered 2d superconductors that we presented earlier.

V. NUMERICAL STUDY OF LDOS FLUCTUATIONS WITH THE ATTRACTIVE HUBBARD MODEL

We consider the attractive- U Hubbard model on the square lattice in two-dimensions with double-periodic boundary conditions. Within the mean-field approximation the Hamiltonian reads ($U > 0$)

$$\hat{H} = -t \sum_{\langle i,j \rangle, \sigma} \hat{c}_{i,\sigma}^\dagger \hat{c}_{j,\sigma} + \sum_{i,\sigma} (V_i - \mu - Un(\mathbf{r}_i)/2) \hat{n}_{i,\sigma} + \sum_i \Delta(\mathbf{r}_i) \hat{c}_{i,\uparrow} \hat{c}_{i,\downarrow} + \text{h.c.} \quad (5)$$

Here $\hat{c}_{j,\sigma}^\dagger$ and $\hat{c}_{j,\sigma}$ stand for the creation and annihilation operators of a fermion with spin projection $\sigma = \pm 1/2$ at a site j . An on-site random potential is drawn from the box distribution, $V_i \in [-W, W]$ with a disorder strength fixed at $W=0.5$ in an attempt to match the experimental disorder strength. The chemical potential μ fixes the filling factor to 0.3. Throughout this work the interaction is taken as $U = 2.2t$ and the system size as $L = 192$, the local occupation number $n(\mathbf{r}_i)$ and the pairing amplitude $\Delta(\mathbf{r}_i)$ are determined self-consistently,

$$n(\mathbf{r}_i) = \sum_{\sigma} \langle \hat{n}_{i,\sigma} \rangle, \quad \Delta(\mathbf{r}_i) = U \langle \hat{c}_{i,\downarrow}^\dagger \hat{c}_{i,\uparrow}^\dagger \rangle, \quad (6)$$

where $\hat{n}_{i,\sigma} = \hat{c}_{i,\sigma}^\dagger \hat{c}_{i,\sigma}$ and the average is taken with respect to the equilibrium density matrix corresponding to the Hamiltonian (5) at zero temperature. We solve Eqs. (5)–(6) iteratively to obtain a self-consistent solution (see Ref. [8] for further computational details). The ensemble averaging involves typically more than a hundred samples and the density of states is computed by averaging on an energy scale $\langle \Delta \rangle / 10$ in good matching with the experimental situation ($\Gamma_{\text{tip}} = 20 \mu\text{eV} \sim \Delta_{\text{SIC}}/10$).

On Figure 5, we show the results of the numerical investigation and compare them with both the analytical theory derived earlier and the experimental results. We check that, as expected at weak disorder and in agreement with the experiment, Δ shows very small fluctuations. On panel **a,b**, we show local density of state maps taken at $E = E_{\max}$ and $E = 2E_{\max}$. Like shown previously on Figure 4 for the experimental results, a strong qualitative difference is observed on the maps. Fluctuations show longer range correlations close to E_{\max} than at higher energy.

A. Normalized variance

Like in the experimental section above, we now proceed to study the normalized variance of the LDOS spatial fluctuations. On panel **c**, we show the mean density of states of the numerical model (black line) along with the normalized variance σ^2 (red). We compare the numerically obtained LDOS variance with the analytical prediction derived from Eq. (4) depending on dimensionless conductance g and dephasing rate γ_Φ . As our tight binding approach considers solutions of the stationary Schrödinger equation, it does not include dephasing. γ_Φ is thus a Thouless energy corresponding to diffusive motion at the scale of system size : $\gamma_\Phi = \frac{\hbar D}{L^2}$. Knowing the density of states and Fermi velocity of the 2d electron gas, we manage to compute Eq.(4) as a function of a single parameter : the dimensionless conductance g (all details are given in Appendix D). We find that $g \sim 10$ reproduce almost perfectly the numerical results (red) on all the energy range we considered. Overall, we show that our field-theoretical analysis, parametrized by g and γ_Φ bridges very well the experimental measurements with the tight-binding model and rationalizes quantitatively the energy-dependent normalized LDOS variance.

B. LDOS distributions

We already know for an experimental fact that disordered systems tend to yield log-normal LDOS distributions [1, 2]. On the theoretical side, scale invariant critical phenomena are known to lead almost universally to log-normal distributions of the density as for instance in the fractionnal Brownian motion . More precisely, close to Anderson transition, a log-normal distribution of the LDOS is expected [9, 13, 15, 16]. Here, we study

the distribution function of both our experimental dI/dV maps and the ones obtained from the attractive Hubbard model. Starting with the numerical results, we plot on Figure 5d, the distribution of the LDOS distribution at fixed energy along with the corresponding (*ie* : of same variance) gaussian and log-normal laws (see Appendix C). A clear log-normal behavior is identified on all the energy range between E_{\max} and $3 E_{\max}$ as confirmed on panel e which compares the RMS deviation of the distribution to either the gaussian or the log-normal model. Turning to the experimental data, we show on Figure 5f, the dI/dV distribution with gaussian (dotted line) and log-normal laws (solid line) of same variance at voltage corresponding to E_{\max} and $1.5 E_{\max}$. Like before, we plot on panel h the RMS deviation to the gaussian or log-normal model. The log-normal model being more accurate is a hint of the multifractal nature of the LDOS fluctuations close to the superconducting coherence peak. We stress that at high energy, a pure log-normal behavior is not expected for the differential conductance dI/dV in contrast with the local density of states (panels d,e) due to the tip height regulation at fixed tunneling current (see Appendix B).

CONCLUSION

As a model system for two-dimensional weakly disordered superconductor where multifractal superconductivity is being actively pursued, we prepared a single monolayer of lead on silicon where electrons are anti-localized in a controlled crystalline disorder and become superconducting below 1.8 K. We report the measurement of tunneling conductance fluctuations with exquisite spatial and spectral resolutions on scales exceeding the superconducting coherence length. To our knowledge, this study is the first to link experimentally spatial LDOS fluctuations with weak anti-localization physics. To support our analysis, we used the attractive Hubbard model with a disorder level finely tuned to match the experiment and probed LDOS fluctuations close to the superconducting coherence peak. Both

experimental and numerical results are shown to be consistent with the mesoscopic fluctuations physics in the weakly anti-localized regime usually probed through transport measurements. The LDOS fluctuation's amplitude depends on two parameters which can be probed and quantitatively extracted in this way: the metal's conductance and an effective electronic dephasing rate.

APPENDIX A : MEAN DENSITY OF STATE

We use the Usadel model [10, 17] to describe the diffusive SIC phase as the mean free path is much smaller than the superconducting coherence length in this sample : $\ell \sim 1nm \ll \xi \sim 50nm$. In more details, we use the spectral angle θ_E parametrisation, with θ_E a solution of an homogenous Usadel equation with a depairing term Γ :

$$iE\sin(\theta_E) + \Delta\cos(\theta_E) - \Gamma\sin(\theta_E)\cos(\theta_E) = 0 \quad (7)$$

The solution of this equation θ_E yields $X_E = \frac{E}{\sqrt{E^2 - \Delta^2}} = \cos(\theta_E)$ from which the density of states $\Re(X_E)$ is obtained.

Using Eq.(8) and Eq.(7), we convolve the density of states of the tip with the one of the sample (along with the Fermi distribution at 300 mK) in order to reproduce the mean differential conductance.

$$I \propto \int \rho_{\text{tip}}(E - eV)\rho_{\text{SIC}}(E, \mathbf{r})(f(E) - f(E - eV))dE \quad (8)$$

where ρ_{tip} and ρ_{SIC} are the respective energy-dependent DOS of the tip and the SIC phase. As detailed on Figure 6, we find that the lead tip is very well described by a Usadel superconductor ($\Delta_{\text{tip}} = 1.345$ meV, $\Gamma_{\text{tip}} = 20\mu\text{eV}$). The SIC phase is found to be very well described by $\Delta_{\text{SIC}} = 0.35$ meV and $\Gamma_{\text{SIC}} = 10\mu\text{eV}$ in excellent agreement with additional measurements using a normal tip (Figure 1b and 6a) and with earlier work [11, 12].

APPENDIX B : DIFFERENTIAL CONDUCTANCE VARIANCE COMPUTATION

We now attempt to rationalise the tunneling conductance spatial fluctuations. Considering a simplified expression for the tunneling current, we write it as a zero temperature convolution of tip and sample density of states Eq.(8). Experimentally, the tip's height above the sample and thus the transmission's coefficient t is not constant but rather controlled by fixing the high voltage current $I(V_\Lambda = 3$ mV) to 2 nA. Trying to estimate density of state leads us to compute:

$$\eta(V, \mathbf{r}) = \frac{\overline{I(V_\Lambda)}}{I(V_\Lambda, \mathbf{r})} \frac{\partial I}{\partial V}(V, \mathbf{r}) \quad (9)$$

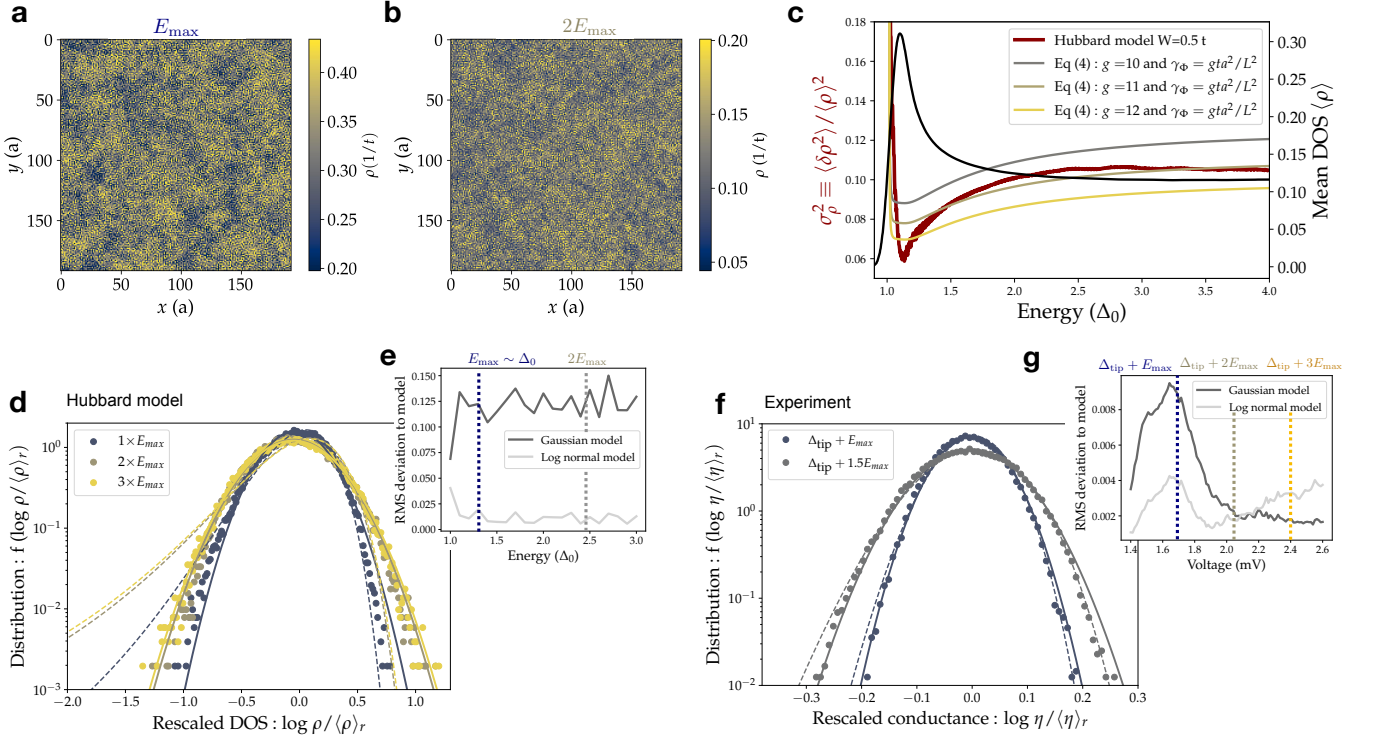


FIG. 5. **Disordered attractive Hubbard model and LDOS distributions** On panel **a,b**, we show local density of state maps taken at $E = E_{\max}$ and $2E_{\max}$ using the attractive Hubbard model. The density of states is given in units of $1/t$ with t the hopping energy. On panel **c**, we show the mean density of states of the numerical model (black line) along with the normalized variance σ^2 (red). We plot analytical prediction from Eq. (4) for $g \in \{10, 11, 12\}$ (see Appendix D for details). We stress that no free parameter has been optimized. On panel **d**, we plot the LDOS distribution at fixed energy along with the corresponding gaussian (dotted line) and log-normal (solid line) distributions (*ie.* of same variance). Distribution functions are given in Appendix C. On panel **e**, we show the RMS deviation to respectively gaussian (dark grey) and log normal (light grey) models. Panels **f,g** are analogous to **d,e** for the experimental dI/dV distribution.

At $T = 0$, we write for the tunneling current I and the tunneling conductance dI/dV :

$$I = |t|^2 \int_0^V dE \rho_{\text{tip}}(E - eV) \rho(E, \mathbf{r}) \quad \text{and} \quad \frac{\partial I}{\partial V} = |t|^2 \rho_{\text{tip}}(0) \rho(V, \mathbf{r}) - |t|^2 \int_0^V dE \rho'_{\text{tip}}(E - V) \rho(E, \mathbf{r}) \quad (10)$$

where $\rho'_{\text{tip}}(E) \equiv d\rho_{\text{tip}}(E)/dE$. It is convenient to introduce the following notations

$$\bar{j}(V) = \int_0^V dE \rho_{\text{tip}}(E - V) \bar{\rho}(E) \quad \text{and} \quad \bar{j}'(V) = \rho_{\text{tip}}(0) \bar{\rho}(V) - \int_0^V dE \rho'_{\text{tip}}(E - V) \bar{\rho}(E) \quad (11)$$

Assuming that fluctuations $\delta\rho(E, \mathbf{r}) = \rho(E, \mathbf{r}) - \bar{\rho}(E)$ near the average DOS $\bar{\rho}(E)$ are weak, we find:

$$\frac{\delta\eta(V, \mathbf{r})}{I(V_\Lambda)} = \frac{\rho_{\text{tip}}(0) \delta\rho(V, \mathbf{r})}{\bar{j}(V_\Lambda)} - \frac{\int_0^\infty dE \delta\rho(E, \mathbf{r}) \rho'_{\text{tip}}(E - V) \bar{j}(V_\Lambda) \Theta(V - E) + \rho_{\text{tip}}(E - V_\Lambda) \bar{j}'(V) \Theta(V_\Lambda - E)}{[\bar{j}(V_\Lambda)]^2} \quad (12)$$

Here $\Theta(x) = 1$, for $x > 0$ and zero otherwise. Hence we obtain

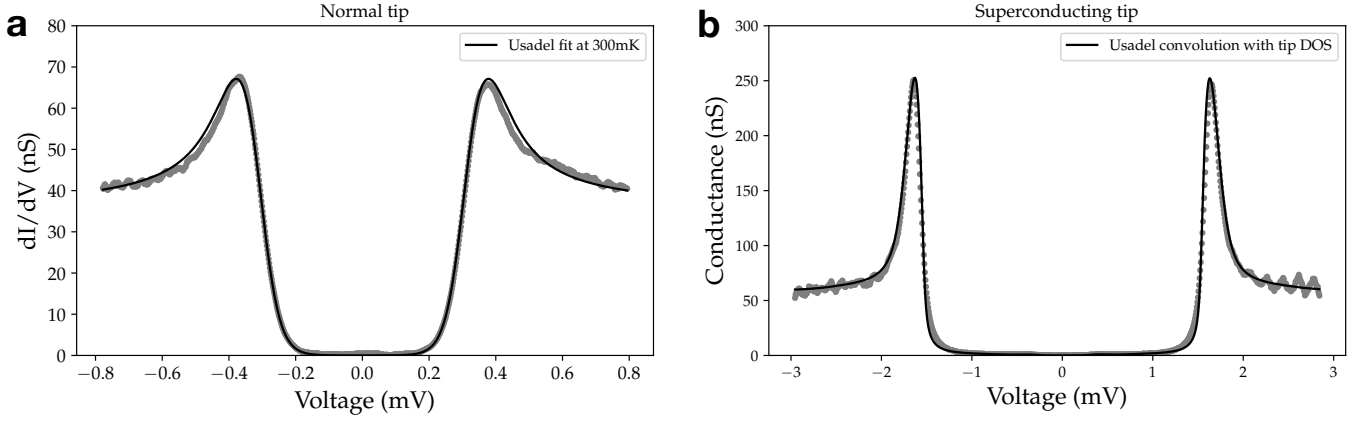


FIG. 6. **Fit of the mean conductance** On **a**, the mean differential conductance measured with a platinum tip is shown as a function of the bias voltage along with the best Usadel fit. On panels **b**, we show the mean dI/dV curve of the large scale spectroscopic map measured with a bulk lead tip while the solid line is a convolution of the Usadel density of states for the sample with the tip density of states at finite temperature.

$$\begin{aligned}
\frac{\langle \delta\eta(V_1, \mathbf{r}_1) \delta\eta(V_2, \mathbf{r}_2) \rangle}{I(V_\Lambda)^2} &= \frac{\rho_{\text{tip}}^2(0)}{\bar{j}(V_\Lambda)\bar{j}(V_\Lambda)} \langle \delta\rho(V_1, \mathbf{r}_1) \delta\rho(V_2, \mathbf{r}_2) \rangle \\
&- \frac{\rho_{\text{tip}}(0)}{\bar{j}(V_\Lambda)} \int_0^\infty dE \langle \delta\rho(V_1, \mathbf{r}_1) \delta\rho(E, \mathbf{r}_2) \rangle \frac{\rho'_{\text{tip}}(E - V_2) \bar{j}(V_\Lambda) \Theta(V_2 - E) + \rho_{\text{tip}}(E - V_\Lambda) \bar{j}'(V_2) \Theta(V_\Lambda - E)}{[\bar{j}(V_\Lambda)]^2} \\
&- \frac{\rho_{\text{tip}}(0)}{\bar{j}(V_\Lambda)} \int_0^\infty dE \langle \delta\rho(V_1, \mathbf{r}_1) \delta\rho(E, \mathbf{r}_2) \rangle \frac{\rho'_{\text{tip}}(E - V_1) \bar{j}(V_\Lambda) \Theta(V_1 - E) + \rho_{\text{tip}}(E - V_\Lambda) \bar{j}'(V_1) \Theta(V_\Lambda - E)}{[\bar{j}(V_\Lambda)]^2} \\
&+ \int_0^\infty dE_1 \int_0^\infty dE_2 \langle \delta\rho(E_1, \mathbf{r}_1) \delta\rho(E_2, \mathbf{r}_2) \rangle \frac{\rho'_{\text{tip}}(E_1 - V_1) \bar{j}(V_\Lambda) \Theta(V_1 - E_1) + \rho_{\text{tip}}(E_1 - V_\Lambda) \bar{j}'(V_1) \Theta(V_\Lambda - E_1)}{[\bar{j}(V_\Lambda)]^2} \\
&\times \frac{\rho'_{\text{tip}}(E_2 - V_2) \bar{j}(V_\Lambda) \Theta(V_2 - E_2) + \rho_{\text{tip}}(E_2 - V_\Lambda) \bar{j}'(V_2) \Theta(V_\Lambda - E_2)}{[\bar{j}(V_\Lambda)]^2}
\end{aligned} \tag{13}$$

APPENDIX C : ISO-ENERGY LDOS DISTRIBUTION

We compare the iso-energy dI/dV distributions to either gaussian or log-normal models of variance σ . The distribution of the logarithm of normalized density of states $x = \log(\rho(E, r)/\langle \rho(E, r) \rangle_r)$ writes for a gaussian distribution :

$$f_{\log-n}(x) = \frac{1}{\sqrt{2\pi\sigma^2}} \exp\left[x - \frac{(e^x - 1)^2}{2\sigma^2}\right] \tag{14}$$

For a log normal distribution which is expected by the sigma-model analysis and recovered in the numerical work, the log of the normalized LDOS x is distributed following :

$$f_n(x) = \frac{1}{\sqrt{2\pi\sigma^2}} \exp\left[-\frac{(x + \sigma^2/2)^2}{2\sigma^2}\right] \tag{15}$$

APPENDIX D : COMPARISON BETWEEN HUBBARD MODEL AND ANALYTICAL DERIVATION

At weak disorder we derive the following result for the local DOS pair correlation function at different energies using Eq.(4) and taking $R = \max(\ell, |\mathbf{r}_1 - \mathbf{r}_2|)$,

$$\langle \delta\rho(E_1, \mathbf{r}) \delta\rho(E_2, \mathbf{r}) \rangle = \frac{\rho_0^2}{4\pi g} \Re \left\{ \left[1 + X_{E_1} X_{E_2}^* \right] \ln \frac{\hbar D / \ell^2}{2E_{\text{Th}} - iE_1 / X_{E_1} + iE_2 / X_{E_2}^*} - \left[1 - X_{E_1} X_{E_2} \right] \ln \frac{\hbar D / \ell^2}{2E_{\text{Th}} - iE_1 / X_{E_1} - iE_2 / X_{E_2}} \right\} \quad (16)$$

where $E_{\text{Th}} = D/(2L^2)$. For this simplified calculation, we used the solution of the Usadel equation that best fitted the Hubbard model mean DOS $\langle \rho(E) \rangle$. For this calculation, we also neglected the imaginary part of X_E , we checked that it has little influence on σ^2 above $1.1\Delta_0$. In order to evaluate Eq. (16) for the attractive Hubbard model, one has to estimate several parameters : g , t/Δ_0 , l/a and γ_Φ/Δ_0 . Once all these parameters are known, we can compute the normalized variance. Fortunately, we see that t and a do not appear explicitly in the final expression. In our numerical solution, we have $\Delta_0/t = 0.12$, following paragraph **c** above, we take $l/a \sim 0.4g$. Following **d** gives $\gamma_\Phi/\Delta_0 = 2.10^{-4}g$. We also have $\hbar D/\ell^2 = 2g\Delta_0/0.12(a/l)^2$

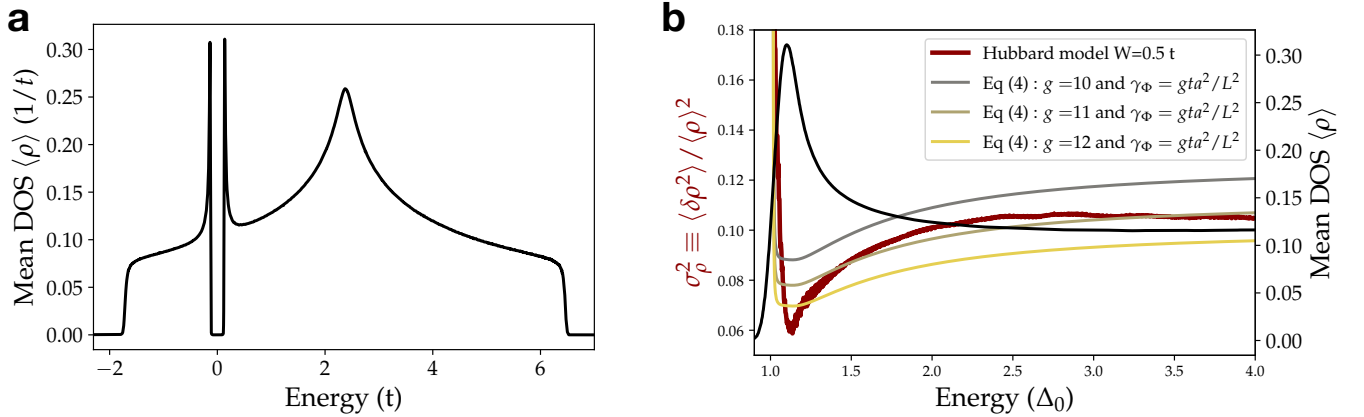


FIG. 7. **Attractive Hubbard model** **a** Mean density of states obtained from self consistent solution of the attractive Hubbard model. **b** Comparison of the normalized variance obtained numerically with the theoretical expectation computed using Eq.(16) for $g \in \{10, 11, 12\}$

-
- [1] A. Richardella, P. Roushan, S. Mack, B. Zhou, D. A. Huse, D. D. Awschalom, and A. Yazdani, *Science* **327**, 665.
- [2] B. Jäck, F. Zinser, E. J. König, S. N. P. Wissing, A. B. Schmidt, M. Donath, K. Kern, and C. R. Ast, *Physical Review Research* **3**, 013022.
- [3] K. Zhao, H. Lin, X. Xiao, W. Huang, W. Yao, M. Yan, Y. Xing, Q. Zhang, Z.-X. Li, S. Hoshino, J. Wang, S. Zhou, L. Gu, M. S. Bahramy, H. Yao, N. Nagaosa, Q.-K. Xue, K. T. Law, X. Chen, and S.-H. Ji, *Nature Physics* **15**, 904.
- [4] B. Sacépé, *Nature Physics* **16**, 13.
- [5] I. S. Burmistrov, I. V. Gornyi, and A. D. Mirlin, *Physical Review B* **92**, 014506 ().
- [6] M. Feigel'man, L. Ioffe, V. Kravtsov, and E. Cuevas, *Annals of Physics* **325**, 1390.
- [7] I. S. Burmistrov, I. V. Gornyi, and A. D. Mirlin, *Physical Review Letters* **108**, 017002 ().
- [8] M. Stosiek, B. Lang, and F. Evers, *Physical Review B* **101**, 144503 ().
- [9] M. Stosiek, F. Evers, and I. S. Burmistrov, arXiv:2107.06728 [cond-mat] (), 2107.06728.
- [10] K. D. Usadel, **25**, 507.
- [11] V. Cherkez, J. Cuevas, C. Brun, T. Cren, G. Ménard, F. Debontridder, V. Stolyarov, and D. Roditchev, *Physical Review X* **4**, 011033.
- [12] C. Brun, T. Cren, V. Cherkez, F. Debontridder, S. Pons, D. Fokin, M. C. Tringides, S. Bozhko, L. B. Ioffe, B. L. Altshuler, and D. Roditchev, *Nature Physics* **10**, 444 ().
- [13] I. S. Burmistrov, I. V. Gornyi, and A. D. Mirlin, arXiv:2101.12713 [cond-mat] (), 2101.12713.
- [14] C. Brun, T. Cren, and D. Roditchev, *Superconductor Science and Technology* **30**, 013003 ().
- [15] I. Lerner, *Physics Letters A* **133**, 253.

- [16] I. S. Burmistrov, I. V. Gornyi, and A. D. Mirlin, *Physical Review B* **93**, 205432 (), 1603.03017.
- [17] S. Gueron, "QUASIPARTICLES IN a DIFFUSIVE CONDUCTOR: INTERACTION AND PAIRING," .